# Photoionization of heliumlike ions with excitation of *nl* states

A. I. Mikhailov and A. V. Nefiodov*

*Theoretical Physics Division, Petersburg Nuclear Physics Institute, 188300 Gatchina, St. Petersburg, Russia*

(Received 9 April 2012; published 17 July 2012)

Photoionization of heliumlike targets accompanied by transition of the residual ions into the arbitrary $nl$ state is studied. The method of nonrelativistic perturbation theory with respect to the interelectron interaction is employed. Cross sections are deduced in the form of universal scalings, which hold for nonrelativistic energies including the near-threshold range. Numerical calculations are compared both with available experimental and with theoretical results.

DOI: 10.1103/PhysRevA.86.013413 PACS number(s): 32.80.Aa, 32.80.Fb

## I. INTRODUCTION

The two-electron transitions in atoms and ions caused by collisions with photons and charged projectiles are intensively studied both theoretically and experimentally in order to get information about the interelectron correlations and multiparticle wave functions [1–3]. The most interesting processes are those which occur entirely due to electron-electron correlations. In the case of photoabsorption, these are double photoionization, photoionization with excitation, and double excitation of a target by a single photon. The majority of experiments are still carried out with neutral helium, which is assumed to be the simplest multielectron atomic system.

Heliumlike multicharged ions with moderate values of nuclear charge $Z$ are even more attractive for investigations of correlated processes, since the corresponding cross sections exhibit the universal scaling behavior. In addition, the theoretical calculations can be performed analytically within the framework of perturbation theory with respect to the interelectron interaction, which appears to be the perturbation theory with respect to the small parameter $1/Z \ll 1$ [4,5]. However, there are also two circumstances which complicate the use of such targets. First, it is still sufficiently difficult to prepare intensive ion beams of high quality. Second, cross sections of the correlated processes decrease rapidly with increasing $Z$ values.

Although the double photoionization of helium has been thoroughly studied, photoionization accompanied by excitation has attracted rather minor attention. The first calculations of the process for the He atom were performed by Brown within the energy range from the ionization threshold to 5 keV [6]. As a wave function of the initial state, the multiparametrical variational function [7] was used. The final state was described as a product of the Coulomb wave functions, which is obviously insufficient in the low-energy regime.

In Refs. [8–10], it was shown that at asymptotically high photon energies $\omega$, the cross section for ionization accompanied by simultaneous excitation of the $nl$ state behaves as $\sigma_{nl}^{+*} \sim \omega^{-7/2-l}$. For $ns$ transitions, this dependence is similar to that of the cross section for a single $K$-shell photoeffect, which decreases as $\sigma^{+} \sim \omega^{-7/2}$ with increasing photon energy. The contributions of transitions into $nl$ states characterized by orbital angular momenta $l \geqslant 1$ decrease more rapidly and, therefore, can be neglected.

At intermediate and low energies, the contribution of excitations into the $nl$ states with $l \geqslant 1$ can be significant. In Ref. [11], the intermediate energy range was considered. As a wave function of the initial state, Drukarev *et al.* used a highly accurate numerical function. The wave function of the final state was constructed as a series expansion with respect to the Sommerfeld parameters $\alpha Zc/v$ and $\alpha c/v$, where $\alpha$ is the fine-structure constant, $c$ is the speed of light, and $v$ is the velocity of the ejected electron. Since the parameter $\alpha Zc$ characterizes the average velocity of a $K$-shell electron, such an expansion is not justified at low energies near the ionization threshold. The cross sections for ionization accompanied by excitation were also calculated for He atoms and for heliumlike ions $Li^{+}$ and $O^{6+}$ at middle and low energies within the framework of sophisticated numerical methods [12–14].

It should be stressed that, in contrast to the high-energy range, the low-energy description of correlated processes in the vicinity of the ionization threshold is a much more complicated problem, because all couplings in the colliding system are essential. Here the electron momenta are of the same order of magnitude as the recoil momentum transferred to the atomic nucleus. Accordingly, one needs to take into account both electron-electron and electron-nucleus interactions consistently. In Refs. [15] and [16], we employed nonrelativistic perturbation theory in the Furry picture. The Coulomb wave and Green's functions were used to the zeroth approximation. The electron-electron interaction was taken into account in both the initial and the final states. The cross sections for photoionization of heliumlike ions accompanied by transitions into the $ns$ and $np$ states were calculated over the entire nonrelativistic range of photon energies.

However, the results in Refs. [15] and [16] contain errors, which are corrected in the present paper. In addition, we make a generalization to the case of excitation of residual ions into arbitrary $nl$ states. The final results are presented in the form of universal scalings, which allow for investigation of most generic features of the correlated process for a wide family of atomic targets. In the following, the conditions $Z \gg 1$ and $\alpha Z \ll 1$ are assumed to be fulfilled. Accordingly, the accuracy of our results is restricted by higher order corrections with respect to the parameters $1/Z$ and $\alpha Z$, which are omitted in the present study. Resonance phenomena near the threshold [17] are not considered here. Relativistic units are used throughout the paper ($\hbar = 1$, $c = 1$).

*anef@thd.pnpi.spb.ru

 

## II. AMPLITUDE OF PHOTOIONIZATION WITH EXCITATION OF THE *nl* STATE

The amplitude of two-electron transition caused by absorption of a single photon reads [5]

$$\mathcal{A} = 2\langle \Psi_f | V_\gamma | \Psi_i \rangle, \tag{1}$$

where $V_\gamma$ is the single-particle operator of the electron-photon interaction and $\Psi_{i,f}(\boldsymbol{r}_1,\boldsymbol{r}_2)$ are the wave functions for the initial and final states of the atomic target. In the nonrelativistic approach, the photon energy $\omega$ is restricted by the condition $\omega \ll m_e$, where $m_e$ is the electron mass. In photoionization processes, the operator $V_\gamma$ can be approximated by the dipole term [18]. Since we shall work in the coordinate representation, the electron-photon interaction is taken in the acceleration form [19,20],

$$V_\gamma(\boldsymbol{r}) = N_\gamma \frac{i\alpha Z}{m_e \omega} \frac{(\mathbf{e}\cdot\boldsymbol{r})}{r^3}, \quad N_\gamma = \frac{\sqrt{4\pi\alpha}}{\sqrt{2\omega}}, \tag{2}$$

where $\mathbf{e}$ is the polarization vector of a photon. Expression (2) is convenient for numerical calculations of the matrix elements, because it improves the convergency of integrals. The wave functions $\Psi_{i,f}(\boldsymbol{r}_1,\boldsymbol{r}_2)$ are found by using the perturbation theory with respect to the electron-electron interaction $V_C(\boldsymbol{r}_1,\boldsymbol{r}_2) = \alpha/|\boldsymbol{r}_1 - \boldsymbol{r}_2|$. To zeroth approximation, the Coulomb wave functions for target with nuclear charge $Z$ are taken. Due to symmetry of the wave functions, amplitude (1) can be represented as the sum of four terms [5],

$$\mathcal{A} = \sqrt{2}(\mathcal{A}_a + \mathcal{A}_b + \mathcal{A}_c + \mathcal{A}_d), \tag{3}$$

where

$$\mathcal{A}_a = \langle \psi_p \psi_{nl} | V_\gamma G(E_a) V_C | \psi_{1s}\psi_{1s}\rangle, \tag{4}$$

$$\mathcal{A}_b = \langle \psi_p \psi_{nl} | V_C G(E_b) V_\gamma | \psi_{1s}\psi_{1s}\rangle, \tag{5}$$

$$\mathcal{A}_c = \langle \psi_{nl} \psi_p | V_\gamma G(E_c) V_C | \psi_{1s}\psi_{1s}\rangle, \tag{6}$$

$$\mathcal{A}_d = \langle \psi_{nl} \psi_p | V_C G(E_b) V_\gamma | \psi_{1s}\psi_{1s}\rangle. \tag{7}$$

Here $G(E)$ denotes the one-particle Coulomb Green's function with energy $E$. The one-electron Coulomb wave functions of the discrete spectrum, $\psi_{1s}$ and $\psi_{nl}$, correspond to the energies $E_1 = -I$ and $E_n = -I/n^2$, respectively, where $I = \eta^2/(2m_e)$, $\eta = m_e\alpha Z$, and $n$ is the principal quantum number. The one-electron Coulomb wave function $\psi_p$ of the continuous spectrum corresponds to the energy $E = p^2/(2m_e)$, where $\boldsymbol{p}$ is the asymptotic momentum of the ejected electron. In Eqs. (4)–(7), the energies of intermediate states are defined as follows:

$$E_a = 2E_1 - E_n, \tag{8}$$

$$E_b = E + E_n - E_1 = \omega + E_1, \tag{9}$$

$$E_c = 2E_1 - E. \tag{10}$$

In Eqs. (9), the second equality results from the energy conservation law $2E_1 + \omega = E + E_n$. Matrix elements (4)–(7) can be represented by four Feynman diagrams (see Fig. 1). Figures 1(a) and 1(c) describe the interaction in the initial state, while Figs. 1(b) and 1(d) account for the interaction in the final state.

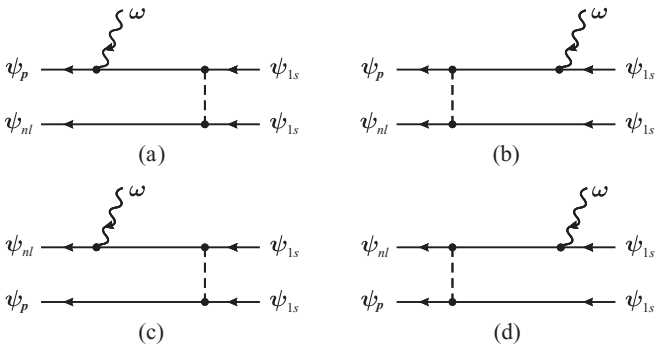


FIG. 1. Feynman diagrams for photoionization with excitation of the *nl* state. Solid lines describe electrons in the Coulomb field of the nucleus.

In Refs. [15] and [16], matrix elements (4)–(7) are calculated in the momentum representation without use of the partial-wave decomposition. The disadvantage of this approach is that the general formulas for excitation of arbitrary *nl* states characterized by different angular momenta $l$ cannot be derived. However, the advantage is that the final formulas are convenient for numerical calculations. In the case of *ns* transitions, the amplitudes can be reduced to single integrals [15], while the amplitudes are given by twofold integrals for *np* transitions [16]. We have found that the formulas obtained in Refs. [15] and [16] contain errors (see Appendix). Therefore, the corresponding numerical results need to be revised.

In the coordinate representation, one can derive the general formulas for transition of the residual ions into the arbitrary final state. However, these formulas contain threefold radial integrals, which require rather time-consuming calculations. In experiments, the cross sections are measured for photoionization with excitation of the whole $n$ shell. Accordingly, one needs to calculate the total cross sections for excitations into all $nl$ subshells. In the following, we work in the coordinate representation, which allows us to separate the radial and angular parts. For example, the wave function $\psi_{nl}(\boldsymbol{r})$ is given by $\psi_{nl}(\boldsymbol{r}) = R_{nl}(r)Y_{lm}(\hat{\boldsymbol{r}})$, where $\hat{\boldsymbol{r}} = \boldsymbol{r}/r$ is the unit vector and $Y_{lm}$ are the spherical harmonics. The radial functions are normalized by the condition

$$\int_0^\infty R_{nl}^2(r) r^2 dr = 1. \tag{11}$$

Since the angular distributions of ejected electrons are not considered here, it is convenient to take the Coulomb wave function $\psi_p$, which is characterized by a definite energy and angular momentum. Namely, $\psi_p(\boldsymbol{r}) = R_{El'}(r)Y_{l'm'}(\hat{\boldsymbol{r}})$, where the radial functions $R_{El}(r)$ are normalized to the $\delta$ function in the energy

$$\int_0^\infty R_{E'l}(r) R_{El}(r) r^2 dr = \delta(E' - E). \tag{12}$$

Then matrix elements (4)–(7) can be cast in the form

$$\mathcal{A}_a = \int \psi_p^*(\boldsymbol{r}_1) V_\gamma(\boldsymbol{r}_1) d\boldsymbol{r}_1 \times \int G(\boldsymbol{r}_1,\boldsymbol{r}_2,E_a) U_n(\boldsymbol{r}_2)\psi_{1s}(\boldsymbol{r}_2) d\boldsymbol{r}_2, \quad (13)$$

$$\mathcal{A}_b = \int \psi_p^*(\boldsymbol{r}_1) U_n(\boldsymbol{r}_1) d\boldsymbol{r}_1 \times \int G(\boldsymbol{r}_1,\boldsymbol{r}_2,E_b) V_\gamma(\boldsymbol{r}_2)\psi_{1s}(\boldsymbol{r}_2) d\boldsymbol{r}_2, \quad (14)$$

$$\mathcal{A}_c = \int \psi_{nl}^*(\boldsymbol{r}_1) V_\gamma(\boldsymbol{r}_1) d\boldsymbol{r}_1 \times \int G(\boldsymbol{r}_1,\boldsymbol{r}_2,E_c) U_p(\boldsymbol{r}_2)\psi_{1s}(\boldsymbol{r}_2) d\boldsymbol{r}_2, \quad (15)$$

$$\mathcal{A}_d = \int \psi_{nl}^*(\boldsymbol{r}_1) U_p(\boldsymbol{r}_1) d\boldsymbol{r}_1 \times \int G(\boldsymbol{r}_1,\boldsymbol{r}_2,E_b) V_\gamma(\boldsymbol{r}_2)\psi_{1s}(\boldsymbol{r}_2) d\boldsymbol{r}_2. \quad (16)$$

Here we have used the following notation:

$$U_n(\boldsymbol{r}) = \int \psi_{nl}^*(\boldsymbol{r}') V_C(\boldsymbol{r}',\boldsymbol{r})\psi_{1s}(\boldsymbol{r}') d\boldsymbol{r}', \quad (17)$$

$$U_p(\boldsymbol{r}) = \int \psi_p^*(\boldsymbol{r}') V_C(\boldsymbol{r}',\boldsymbol{r})\psi_{1s}(\boldsymbol{r}') d\boldsymbol{r}'. \quad (18)$$

Expanding the operator $V_C$ of the electron-electron interaction over the spherical harmonics yields

$$U_n(\boldsymbol{r}) = \frac{4\pi\alpha}{2l+1} u_{nl}(r) Y_{lm}^*(\hat{\boldsymbol{r}}), \quad (19)$$

$$u_{nl}(r) = \int_0^\infty \Lambda_l(r,r') R_{nl}(r')\psi_{1s}(r') r'^2 dr', \quad (20)$$

$$U_p(\boldsymbol{r}) = \frac{4\pi\alpha}{2l'+1} u_{El'}(r) Y_{l'm'}^*(\hat{\boldsymbol{r}}), \quad (21)$$

$$u_{El}(r) = \int_0^\infty \Lambda_l(r,r') R_{El}(r')\psi_{1s}(r') r'^2 dr', \quad (22)$$

where $\Lambda_l(r,r') = r_<^l / r_>^{l+1}$, $r_< = \min\{r,r'\}$, and $r_> = \max\{r,r'\}$. The partial-wave decomposition for the Coulomb Green's function is given by

$$G(\boldsymbol{r}_1,\boldsymbol{r}_2,E) = \sum_{\lambda,\mu} G_\lambda(r_1,r_2,\nu) Y_{\lambda\mu}^*(\hat{\boldsymbol{r}}_1) Y_{\lambda\mu}(\hat{\boldsymbol{r}}_2), \quad (23)$$

where $\nu = \eta/\sqrt{-(2m_e E + i0)}$.

For simplicity, we chose the spherical basis vector $\mathbf{e}_0 = \mathbf{e}_z$ as the polarization vector $\mathbf{e}$. Then, after integration over angles in Eqs. (13)–(16), the expression for total amplitude (3) reads

$$\mathcal{A} = \frac{i\alpha Z}{3m_e}\left(\frac{4\pi\alpha}{\omega}\right)^{3/2} C^{10}_{l0\,l'0} C^{10}_{lm\,l'm'} \times \left\{\frac{\Pi_{l'}}{\Pi_l}(J_a + J_b) + \frac{\Pi_l}{\Pi_{l'}}(J_c + J_d)\right\}, \quad (24)$$

where $\Pi_l = \sqrt{2l+1}$ and the standard notations for the Clebsch-Gordan coefficients are used. In Eq. (24), the radial integrals take the form

$$J_a = \int_0^\infty R_{El'}(r_1) dr_1 \int_0^\infty G_l(r_1,r_2,\nu_a) u_{nl}(r_2)\psi_{1s}(r_2) r_2^2 dr_2, \quad (25)$$

$$J_b = \int_0^\infty R_{El'}(r_1) u_{nl}(r_1) r_1^2 dr_1 \int_0^\infty G_1(r_1,r_2,\nu_b)\psi_{1s}(r_2) dr_2, \quad (26)$$

$$J_c = \int_0^\infty R_{nl}(r_1) dr_1 \int_0^\infty G_{l'}(r_1,r_2,\nu_c) u_{El'}(r_2)\psi_{1s}(r_2) r_2^2 dr_2, \quad (27)$$

$$J_d = \int_0^\infty R_{nl}(r_1) u_{El'}(r_1) r_1^2 dr_1 \int_0^\infty G_1(r_1,r_2,\nu_b)\psi_{1s}(r_2) dr_2. \quad (28)$$

For derivation of the universal scalings, it is convenient to use the dimensionless variable $x = \eta r$ and to express all momenta and energies in units of $\eta$ and $I$, respectively. Then the dimensionless asymptotic momentum $k$ of the ejected electron is given by $k = p/\eta$, while the corresponding dimensionless energy is just $\varepsilon = E/I = \xi^{-2}$, where $\xi = 1/k$. The dimensionless photon energy is defined as $\varepsilon_\gamma = \omega/I$. The energy-conservation law for the process under consideration takes the form $\varepsilon_\gamma = \xi^{-2} + 2 - n^{-2}$.

The radial parts of the Coulomb wave functions are given by

$$R_{nl}(r) = \eta_n^{3/2}\mathcal{R}_{nl}(x), \quad (29)$$

$$\mathcal{R}_{nl}(x) = N_{nl}\rho^l e^{-x/n} F(l+1-n, 2l+2, \rho), \quad (30)$$

$$R_{El}(r) = \sqrt{\eta m_e}\,\mathcal{R}_{\varepsilon l}(x), \quad (31)$$

$$\mathcal{R}_{\varepsilon l}(x) = N_{\varepsilon l}\zeta^l e^{-ikx} F(l+1+i\xi, 2l+2, i\zeta), \quad (32)$$

where $\eta_n = \eta/n$, $\rho = 2x/n$, $\zeta = 2kx$, and $F(a,b,z)$ is the regular confluent hypergeometric function. In Eqs. (30) and (32), the normalization factors are defined as follows:

$$N_{nl} = \frac{2}{\Gamma(2l+2)}\frac{\sqrt{\Gamma(l+1+n)}}{\sqrt{n\Gamma(n-l)}}, \quad (33)$$

$$N_{\varepsilon l} = \frac{\sqrt{2}}{\sqrt{\pi\xi}} e^{\pi\xi/2}\frac{|\Gamma(l+1-i\xi)|}{\Gamma(2l+2)}, \quad (34)$$

where $\Gamma(z)$ is Euler's $\Gamma$ function.

The radial part of Green's function is given by

$$G_\lambda(r_1,r_2,\nu) = \eta m_e\,\mathcal{G}_\lambda(x_1,x_2,\nu), \quad (35)$$

$$\mathcal{G}_\lambda(x_1,x_2,\nu) = \frac{\nu\Gamma(\lambda+1-\nu)}{\Gamma(2\lambda+2)x_1x_2} M_{\nu,\mu}(\kappa_<) W_{\nu,\mu}(\kappa_>), \quad (36)$$

where $\mu = \lambda + 1/2$, $\kappa_{\lessgtr} = 2x_{\lessgtr}/\nu$, $x_< = \min\{x_1,x_2\}$, and $x_> = \max\{x_1,x_2\}$. The Whittaker functions, $M_{\nu,\mu}$ and $W_{\nu,\mu}$, are defined as [21]

$$M_{\nu,\mu}(z) = e^{-z/2} z^{\lambda+1} F(\lambda+1-\nu, 2\lambda+2, z), \quad (37)$$

$$W_{\nu,\mu}(z) = e^{-z/2} z^{\lambda+1} \Psi(\lambda+1-\nu, 2\lambda+2, z), \quad (38)$$

where $\Psi(a,b,z)$ is the irregular confluent hypergeometric function.

Functions (20) and (22) can be written as

$$u_{nl}(r) = \frac{\eta_n}{\sqrt{n\pi}}\, w_{nl}(x), \tag{39}$$

$$w_{nl}(x) = \int_0^\infty \Lambda_l(x,x')\mathcal{R}_{nl}(x')e^{-x'}x'^2dx', \tag{40}$$

$$u_{El}(r) = \frac{\sqrt{m_e}}{\sqrt{\pi}}\, w_{\varepsilon l}(x), \tag{41}$$

$$w_{\varepsilon l}(x) = \int_0^\infty \Lambda_l(x,x')\mathcal{R}_{\varepsilon l}(x')e^{-x'}x'^2dx'. \tag{42}$$

Finally, total amplitude (24) takes the form

$$\mathcal{A} = \frac{i\alpha Z}{3\pi m_e}\left(\frac{4\pi\alpha m_e}{n\omega}\right)^{3/2} C^{10}_{l0l'0}C^{10}_{lml'm'}D_{ll'}. \tag{43}$$

Here

$$D_{ll'} = \frac{\Pi_{l'}}{\Pi_l}(\mathcal{J}_a + \mathcal{J}_b) + \frac{\Pi_l}{\Pi_{l'}}(\mathcal{J}_c + \mathcal{J}_d), \tag{44}$$

$$\mathcal{J}_a = \int_0^\infty \mathcal{R}_{\varepsilon l'}(x_1)dx_1 \int_0^\infty \mathcal{G}_l(x_1,x_2,\nu_a)w_{nl}(x_2)e^{-x_2}x_2^2dx_2, \tag{45}$$

$$\mathcal{J}_b = \int_0^\infty \mathcal{R}_{\varepsilon l'}(x_1)w_{nl}(x_1)x_1^2dx_1 \int_0^\infty \mathcal{G}_1(x_1,x_2,\nu_b)e^{-x_2}dx_2, \tag{46}$$

$$\mathcal{J}_c = \int_0^\infty \mathcal{R}_{nl}(x_1)dx_1 \int_0^\infty \mathcal{G}_{l'}(x_1,x_2,\nu_c)w_{\varepsilon l'}(x_2)e^{-x_2}x_2^2dx_2, \tag{47}$$

$$\mathcal{J}_d = \int_0^\infty \mathcal{R}_{nl}(x_1)w_{\varepsilon l'}(x_1)x_1^2dx_1 \int_0^\infty \mathcal{G}_1(x_1,x_2,\nu_b)e^{-x_2}dx_2, \tag{48}$$

where $\nu_a = 1/\sqrt{2-n^{-2}}$, $\nu_b = i/\sqrt{\varepsilon+1-n^{-2}}$, and $\nu_c = 1/\sqrt{\varepsilon+2}$. Integrals (25)–(28) and (45)–(48) are related to each other via the following equality:

$$J_i = \frac{1}{\pi}\left(\frac{m_e}{n}\right)^{3/2}\mathcal{J}_i, \quad (i = a,\ldots,d). \tag{49}$$

## III. CROSS SECTION FOR PHOTOIONIZATION WITH EXCITATION OF THE *nl* STATE

The cross section for the process under consideration reads

$$\sigma^{+*}_{nl} = 2\pi \sum_{l',m',m} |\mathcal{A}|^2, \tag{50}$$

where amplitude $\mathcal{A}$ is given by Eq. (43). Taking into account that

$$\sum_{m,m'} \left(C^{10}_{lml'm'}\right)^2 = 1, \tag{51}$$

one obtains the universal scaling

$$\sigma^{+*}_{nl} = \frac{2^{10}\pi\sigma_0}{9Z^4n^3}\, Q_{nl}(\xi), \tag{52}$$

$$Q_{nl}(\xi) = \varepsilon_\gamma^{-3} \sum_{l'=|l-1|}^{l+1} \left|C^{10}_{l0l'0}D_{ll'}\right|^2. \tag{53}$$

Here $\sigma_0 = \alpha\pi a_0^2 \simeq 0.642$ Mb, $a_0 = 1/(m_e\alpha)$ is the Bohr radius, $\varepsilon = \xi^{-2}$, $\varepsilon_\gamma = \xi^{-2} + 2 - n^{-2}$, and $D_{ll'}$ is given by Eq. (44). Formula (52) is valid over the entire nonrelativistic energy range characterized by $2 - n^{-2} \leqslant \varepsilon_\gamma \ll 2(\alpha Z)^{-2}$.

The function $Q_{nl}(\xi)$ does not depend on the value of $Z$, being the universal one for a whole sequence of heliumlike ions. At high and low energies, it can be expanded in parameters $\xi$ and $\xi^{-1}$, respectively. In the case of excitations into $ns$ states, we have found two leading terms of these expansions, which read

$$Q_{ns}(\xi) \simeq \begin{cases} B_1 - B_2\xi^{-2} & \text{if } \xi \gg 1, \\ \dfrac{\xi^8}{e^{2\pi\xi}-1}(C_1 - C_2\xi^2) & \text{if } \xi \ll 1. \end{cases} \tag{54}$$

Note that we do not make an expansion with respect to the parameter $\pi\xi$, which is not supposed to be small. The expansion coefficients for different values of the principal quantum number $n$ are listed in Table I. As can be seen, the second coefficients are always larger than the first ones.

The ratio of the cross section for the process under consideration to that for a single photoeffect is also of experimental interest. The nonrelativistic cross section for $K$-shell photoionization of heliumlike ions is known in analytical form [22],

$$\sigma^+ = \frac{2^{10}\pi\sigma_0}{3Z^2\varepsilon_\gamma^4}\,\frac{e^{-4\tau\,\mathrm{arccot}\,\tau}}{(1-e^{-2\pi\tau})}, \tag{55}$$

where $\tau = 1/\sqrt{\varepsilon_\gamma - 1}$. Then the ratio of cross sections is given by

$$R_{nl} = \frac{\sigma^{+*}_{nl}}{\sigma^+} = \frac{H_{nl}(\xi)}{Z^2n^3}, \tag{56}$$

$$H_{nl}(\xi) = \frac{\varepsilon_\gamma^4}{3}\,\frac{(1-e^{-2\pi\tau})}{e^{-4\tau\,\mathrm{arccot}\,\tau}}\, Q_{nl}(\xi). \tag{57}$$

TABLE I. Expansion coefficients in Eq. (54) and limiting values for functions $H_{nl}(\xi)$.

| $n$ | $10^2 \times B_1$ | $10 \times B_2$ | $C_1$ | $C_2$ | $H_{ns}(\xi)$ $(\xi \to 0)$ | $H_{ns}(\xi)$ $(\xi \to \infty)$ | $H_{np}(\xi)$ $(\xi \to \infty)$ | $H_{nd}(\xi)$ $(\xi \to \infty)$ |
|---|---|---|---|---|---|---|---|---|
| 2 | 1.578 | 0.332 | 2.1864 | 7.008 | 0.729 | 1.332 | 0.967 | |
| 3 | 0.916 | 0.188 | 1.3824 | 5.208 | 0.461 | 0.959 | 0.861 | 0.0195 |
| 4 | 0.770 | 0.157 | 1.1952 | 4.728 | 0.399 | 0.867 | 0.831 | 0.0243 |
| 5 | 0.713 | 0.145 | 1.1208 | 4.536 | 0.374 | 0.829 | 0.818 | 0.0263 |
| 6 | 0.684 | 0.139 | 1.0824 | 4.428 | 0.361 | 0.810 | 0.812 | 0.0273 |
| 7 | 0.667 | 0.136 | 1.0596 | 4.368 | 0.353 | 0.798 | 0.808 | 0.0279 |
| 8 | 0.656 | 0.133 | 1.0464 | 4.332 | 0.349 | 0.791 | 0.805 | 0.0283 |

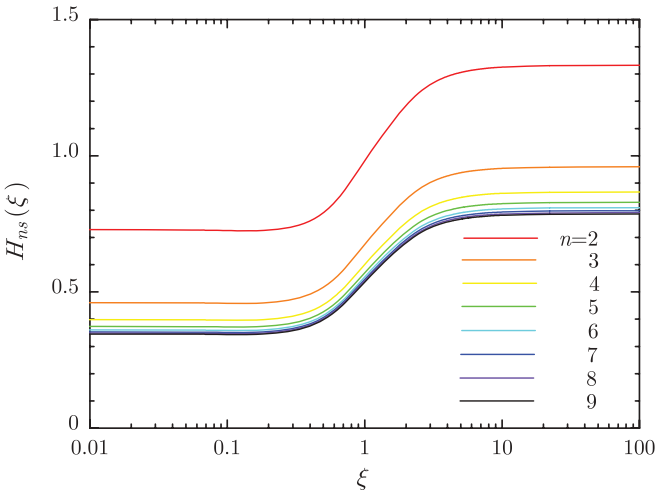


FIG. 2. (Color online) Functions $H_{ns}(\xi)$ with dependence on the parameter $\xi$ for the principal quantum numbers $n \geqslant 2$. In Figs. 2–5, all curves are numbered in order with use of the same colors for the same $n$ values.

We have calculated the universal functions $H_{nl}(\xi)$ with dependence on the parameter $\xi$ for transitions into the $ns$, $np$, and $nd$ states (see Figs. 2–4). The quality of numerical calculations has been checked by using different gauges (in the acceleration, length, and velocity forms), as well as by using the corrected formulas obtained in Refs. [15] and [16] for the case of $ns$ and $np$ excitations. Within the high-energy domain ($\xi \ll 1$), only transitions into $ns$ states contribute to the cross section. The contributions from excitation of other states with $l \geqslant 1$ tend to 0 when $\xi \to 0$. Within the near-threshold energy domain ($\xi \gg 1$), all the cross sections peak. However, cross sections $\sigma_{nd}^{+*}$ turn out to be too small in comparison to those for excitation of $ns$ and $np$ states. In general, with increasing values of $l$, the cross sections for excitation of $nl$ states decrease rapidly when $l > 1$. The limiting values of functions $H_{nl}(\xi)$ both at the threshold and at asymptotic high energies are listed in Table I. For $n > 7$, the functions $H_{nl}(\xi)$ become practically $n$ independent. The range of fast changes in $H_{nl}(\xi)$ lies at intermediate energies $\xi \sim 1$.

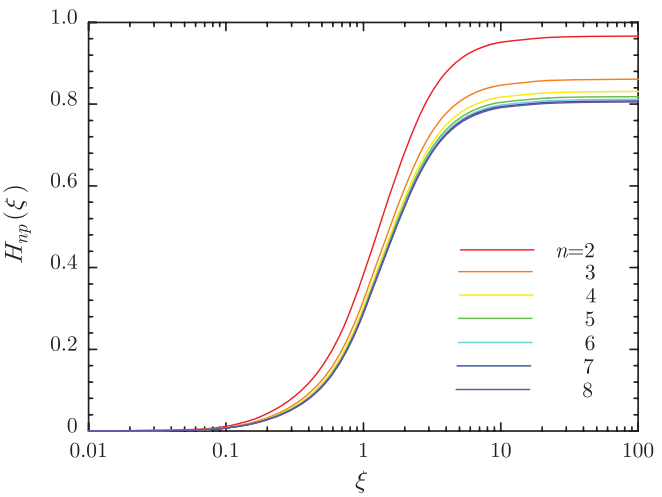


FIG. 3. (Color online) Functions $H_{np}(\xi)$ vs $\xi$ for $n \geqslant 2$.

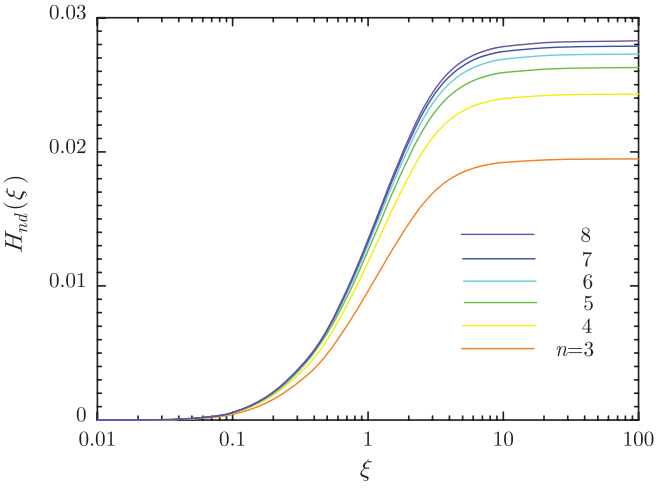


FIG. 4. (Color online) Functions $H_{nd}(\xi)$ vs $\xi$ for $n \geqslant 3$.

Since the dominant excitation channels are due to transitions into $ns$ and $np$ states, we have also depicted the curves for the cross-section ratio $\chi_n(\xi) = \sigma_{np}^{+*}/\sigma_{ns}^{+*} = R_{np}/R_{ns}$ dependent on the parameter $\xi$ for different values of $n$. As shown in Fig. 5, for $\xi \gtrsim 5$ and $n > 3$, the function $\chi_n(\xi)$ is close to 1. Note that these results are in disagreement with the calculations made for $Li^+$ ions within the near-threshold energy range [14], where the cross sections $\sigma_{np}^{+*}$ are already larger than $\sigma_{ns}^{+*}$ for $n = 2$. The discrepancy could be caused by higher-order correlation corrections with respect to the parameter $1/Z$, which are not considered here.

In Fig. 6, we compare separate contributions of the Feynman diagrams to $H_{2s}(\xi)$ and $H_{2p}(\xi)$. The qualitative behavior of these contributions depending on the variable $\xi$ remains similar for other values of $n > 2$ also. The numerical calculations are performed by using the velocity gauge. Excitation of the $2s$ state appears to be due mainly to the diagram depicted in Fig. 1(a), which describes the interelectron interaction in the initial state. At high energies, this is the only contribution to the process under consideration [10]. The other diagrams become noticeable at $\xi \gtrsim 0.5$. Note that the diagram in Fig. 1(c) turns out to be negligibly small, although there is

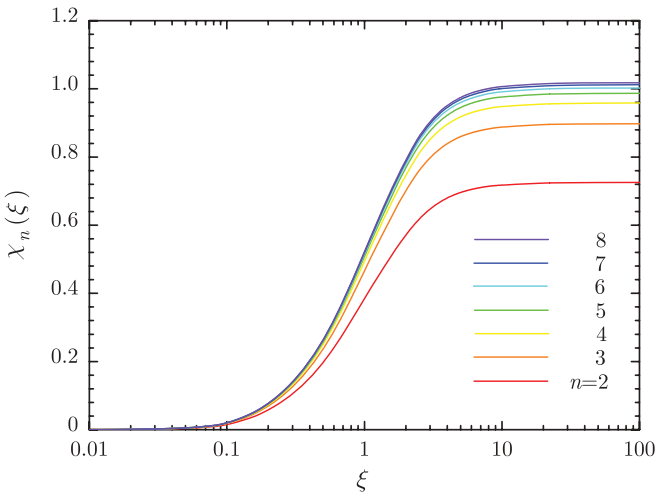


FIG. 5. (Color online) Functions $\chi_n(\xi) = \sigma_{np}^{+*}/\sigma_{ns}^{+*}$ vs $\xi$ for $n \geqslant 2$.

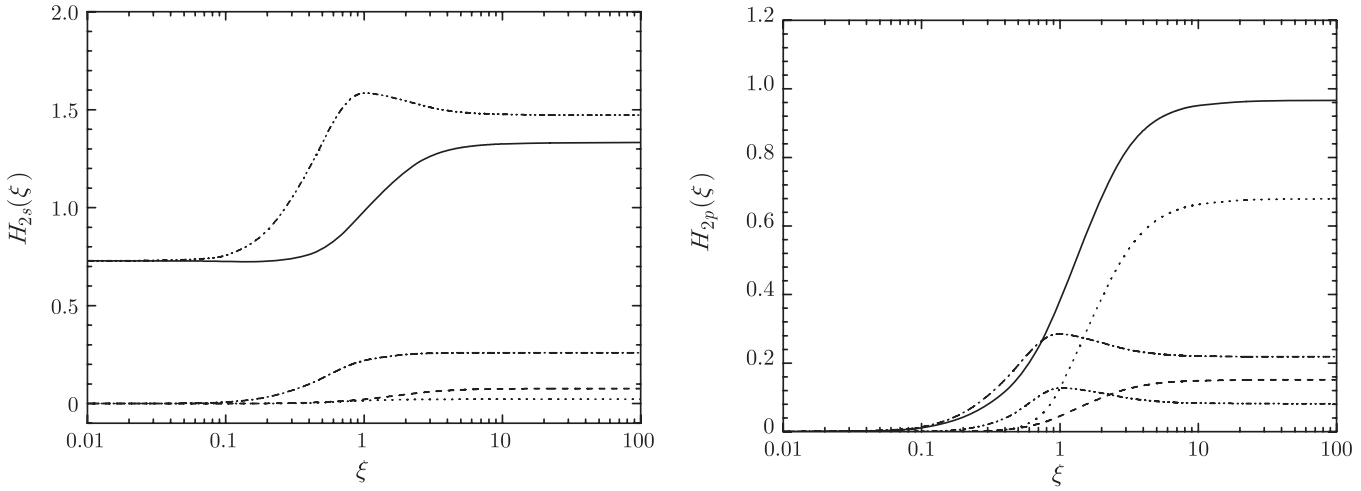


FIG. 6. Contributions of the separate Feynman diagrams to $H_{2s}(\xi)$ and $H_{2p}(\xi)$ in the velocity gauge. Dash-dot-dotted, dash-dotted, dotted, and dashed curves correspond to the contributions of the diagrams in Figs. 1(a), 1(b), 1(c), and 1(d), respectively. The solid line is the total contribution of all diagrams.

no explicit parametrical smallness. In contrast to that, in the case of $2p$ excitation, this diagram gives rise to the dominant contribution within the near-threshold energy domain, while at the energy range characterized by $0.1 \lesssim \xi \lesssim 1$ the dominant contribution appears from the diagram in Fig. 1(b), which accounts for the interelectron interaction in the final state.

It should be noted that gauge-invariant results are obtained only if the total contribution of all four diagrams is calculated taking into account the interference terms (see Fig. 7). Although these terms can contribute significantly to the cross sections of correlated processes, they are often unreasonably disregarded in different model calculations (see, e.g., Refs. [23–26]). In Fig. 7, we also compare the exact calculations with approximation (54). As can be seen, both high- and low-energy expansions already fail to converge at the intermediate range $\xi \sim 1$.

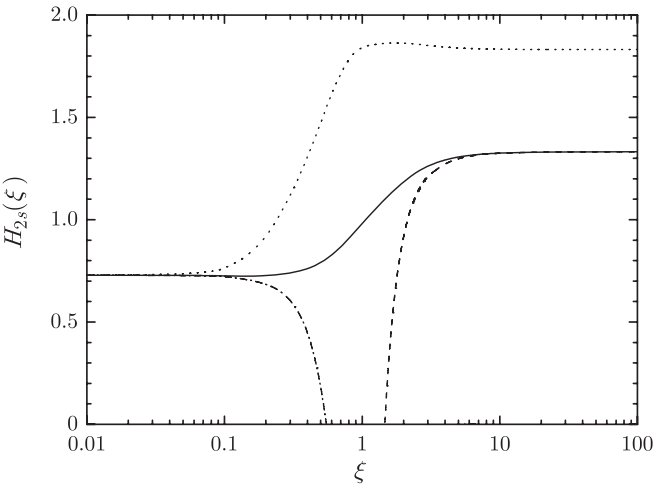


FIG. 7. Function $H_{2s}(\xi)$ as a coherent (solid line) and an incoherent (dotted line) sum of the contributions of the four Feynman diagrams in Fig. 1. Approximations by Eq. (54) at high and low energies are shown by the dash-dotted and dashed curves, respectively.

The quantities of experimental interest are the cross sections for ionization with excitation of residual ions into the whole $n$ shell $\sigma_n^{+*} = \sum_{l=0}^{n-1} \sigma_{nl}^{+*}$ and the corresponding cross-section ratios $R_n = \sigma_n^{+*}/\sigma^+ = \sum_{l=0}^{n-1} R_{nl}$. Up to now the measurements are available for helium atoms only. Since, in the perturbation theory we employ, the small parameter is assumed to be $1/Z \ll 1$, our results for helium are not supposed to be accurate enough. However, due to the fast convergency of the

TABLE II. Comparison of experimental (top rows, from Ref. [27]) and theoretical (middle rows, from Ref. [13]; lower rows, present work) results for the ratio $R_n = \sigma_n^{+*}/\sigma^+$ in helium.

| $\omega$ (eV) | $R_2$ (%) | $R_3$ (%) | $R_4$ (%) | $R_5$ (%) | $R_6$ (%) |
|---|---|---|---|---|---|
| 89.5 | 8.17(4) | 1.51(3) | 0.57(6) | 0.284(28) | 0.168(25) |
| | 7.69 | 1.45 | 0.570 | 0.295 | 0.165 |
| | 5.29 | 1.31 | 0.530 | 0.268 | 0.154 |
| 100.0 | 7.63(4) | 1.38(3) | 0.53(5) | 0.264(25) | 0.147(22) |
| | 7.16 | 1.27 | 0.486 | 0.238 | 0.141 |
| | 4.84 | 1.16 | 0.464 | 0.233 | 0.133 |
| 120.0 | 6.96(5) | 1.16(3) | 0.41(4) | 0.193(20) | 0.106(20) |
| | 6.67 | 1.12 | 0.418 | 0.202 | 0.106 |
| | 4.26 | 0.977 | 0.384 | 0.191 | 0.109 |
| 160.0 | 6.39(10) | 0.96(4) | 0.35(4) | 0.139(20) | 0.075(20) |
| | 6.19 | 0.935 | 0.333 | 0.160 | 0.090 |
| | 3.62 | 0.787 | 0.303 | 0.149 | 0.085 |
| 220.0 | 5.68(15) | 0.86(4) | 0.29(2) | 0.132(20) | |
| | 5.78 | 0.831 | 0.288 | 0.137 | 0.077 |
| | 3.16 | 0.657 | 0.249 | 0.122 | 0.069 |
| 300.0 | 5.48(10) | 0.736(45) | 0.232(20) | 0.099(20) | |
| | 5.55 | 0.767 | 0.264 | 0.123 | 0.067 |
| | 2.86 | 0.578 | 0.217 | 0.106 | 0.059 |
| 389.9 | 5.43(15) | 0.690(45) | 0.207(20) | 0.095(20) | |
| | 5.38 | 0.726 | 0.248 | 0.115 | 0.064 |
| | 2.69 | 0.534 | 0.199 | 0.096 | 0.054 |
| 499.1 | 5.22(15) | 0.731(60) | 0.188(20) | | |
| | 5.25 | 0.695 | 0.235 | 0.110 | 0.066 |
| | 2.58 | 0.504 | 0.187 | 0.090 | 0.051 |

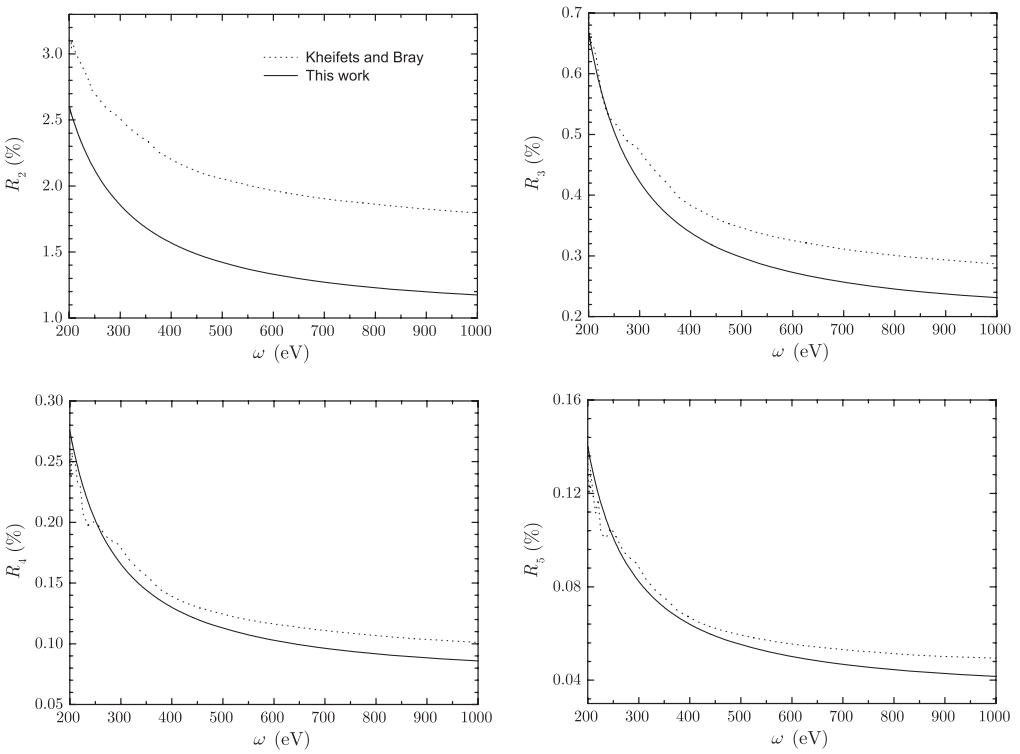


FIG. 8. Cross-section ratio $R_n$ for photoionization of $Li^+$ ions with simultaneous excitation of the $n$ shell. Calculations performed by Kheifets and Bray [13] using a gauge in the acceleration form are given for comparison.

series expansion over the correlation parameter $1/Z$ [5,18], cross section (52) is expected to be correct by an order of magnitude even for targets with small values of $Z \gtrsim 1$. The most significant contribution should arise from the Feynman diagrams of two-photon exchange.

In Table II, we compare the theoretical predictions for the cross-section ratios $R_n$ at different $n$ and photon energies $\omega$ with experimental data of Wehlitz *et al.* [27]. For each photon energy, the top row of numbers indicates the experimental results, with the experimental errors in parentheses; the middle row of numbers is obtained within the framework of the convergent close-coupling approach [13] using the gauge in acceleration form; and the lower row of numbers is the results of our calculations. Note that within the near-threshold energy range, the results of Ref. [13] exhibit a slight gauge dependence, about 2%. In addition, the cross sections $\sigma_n^{+*}$ calculated by using the gauge in the length form have incorrect high-energy asymptotic behavior (see Fig. 10 in Ref. [13]). Except for the case of $n = 2$, our results are in satisfactory agreement both with numerical calculations performed within the framework of the convergent close-coupling formalism and with experimental measurements. Since in the lowest order of perturbation theory the Coulomb binding energy differs significantly from the experimental value for helium atom, theory and experiment are compared at the same energy of ejected electron. More specifically, for a given value of photon energy $\omega$, we calculate the energy $E = \omega - I_n^{+*}$ of the ejected electron, which is used as the input parameter in theoretical calculations, that is, dimensionless quantities $\varepsilon = \xi^{-2}$ and $\varepsilon_\gamma = \varepsilon + 2 - n^{-2}$ are defined via the excess energy $E$. Here $I_n^{+*}$ denotes the threshold energy, which is overadjusted by higher-order correlation corrections:

$$I_n^{+*} = I\left(\sum_{k\geqslant 0} \epsilon_k Z^{-k} - n^{-2}\right), \tag{58}$$

where $I = m_e(\alpha Z)^2/2$, $\epsilon_0 = 2$, $\epsilon_1 = -5/4$, $\epsilon_2 = 0.3153$, and $\epsilon_3 = -0.0174$ [28]. Formula (58) reproduces the experimental energies for heliumlike targets with small values of $Z \gtrsim 1$. To be consistent, in general, one needs to deduce the cross sections at the same level of accuracy, taking into account higher-order terms of perturbation theory. However, this problem is presently not solved. For particular values of the photon energy $\omega$, the parameter $\xi$ depends on $n$. For example, in helium, where $I = 54.4$ eV, at $\omega = 89.5$ eV one gets $\xi = 1.502$ for $n = 2$ and $\xi = 2.128$ for $n = 6$. If $\omega = 499.1$ eV, we have $\xi = 0.354$ for $n = 2$ and $\xi = 0.359$ for $n = 6$.

TABLE III. Comparison of cross sections $\sigma_n^{+*}$ calculated within the framework of the convergent close-coupling approach [13] (top rows) for the heliumlike ion $O^{6+}$ with numerical results of the present work (bottom rows).

| $\omega$ (eV) | $\sigma_2^{+*}$ (b) | $\sigma_3^{+*}$ (b) | $\sigma_4^{+*}$ (b) | $\sigma_5^{+*}$ (b) | $\sigma_6^{+*}$ (b) |
|---|---|---|---|---|---|
| 1688.97 | 109 | 26.4 | 9.87 | 4.49 | 2.20 |
| | 89.6 | 22.6 | 9.25 | 4.69 | 2.70 |
| 1939.00 | 65.9 | 14.5 | 5.40 | 2.44 | 1.18 |
| | 53.8 | 12.9 | 5.16 | 2.59 | 1.48 |
| 3738.96 | 6.36 | 1.24 | 0.460 | 0.220 | 0.121 |
| | 5.61 | 1.17 | 0.446 | 0.218 | 0.123 |
| 5738.96 | 1.48 | 0.281 | 0.103 | 0.049 | 0.028 |
| | 1.37 | 0.275 | 0.103 | 0.050 | 0.028 |

In Fig. 8, we have presented the cross-section ratios $R_n$ for photoionization of heliumlike ion $Li^+$ with simultaneous excitation of the $n$ shell. In this case, the threshold energy is given by Eq. (58), where $I = 122.45$ eV. The photon energy range is chosen to be $200 \leqslant \omega \leqslant 1000$ eV. At $\omega = 200$ eV one gets $\xi = 1.940$ for $n = 2$ and $\xi = 4.242$ for $n = 5$. If $\omega = 1$ keV, we have $\xi = 0.384$ for $n = 2$ and $\xi = 0.390$ for $n = 5$. Except for the case of $n = 2$, our results are in satisfactory agreement with numerical calculations performed within the framework of the convergent close-coupling approach [13]. The discrepancy can be explained by higher-order correlation corrections, which are omitted here.

In Table III, we compare the cross sections $\sigma_n^{+*}$ obtained by Kheifets and Bray [13] for the heliumlike ion $O^{6+}$ with our numerical calculations. Again, the most significant disagreement of the results is observed for excitations of the $n = 2$ shell.

## IV. SUMMARY

We have deduced formulas for the cross sections of photoionization of heliumlike ions accompanied by simultaneous excitation of the residual ions into the $nl$ state. The method of nonrelativistic perturbation theory with respect to the interelectron interaction is used. The study is performed for atomic targets characterized by small parameters $1/Z \ll 1$ and $\alpha Z \ll 1$. In addition, the dipole approximation is employed, that is, the dimensionless photon momentum (nondipolarity parameter) $\varkappa = \alpha Z \varepsilon_\gamma/2$ is assumed to be negligibly small [5,18]. Accordingly, the accuracy of our predictions is restricted by corrections of the order $1/Z$ and $\alpha Z$, which are not taken into account in this work.

The cross sections exhibit the universal scaling behavior over both the nuclear charge $Z$ and the principal quantum number $n$, when $n > 7$. At low energies near the ionization threshold, the cross sections of the $ns$ and $np$ excitations are comparable by magnitude, while the transitions into the $nd$ states are smaller by two orders of magnitude. The present results are in satisfactory agreement both with measurements made on neutral helium [27] and with numerical calculations performed within the framework of the convergent close-coupling approach for He, $Li^+$, and $O^{6+}$ targets [13]. The only exception is the particular case of $n = 2$ excitations, where the Feynman diagrams of two-photon exchange should be taken into account.

In some experiments [23,24], the cross sections for double $K$-shell photoionization of neutral atoms are determined via measurements of the yield of x-ray photons emitted at filling of the empty $K$ shell. In this case, the total cross section is given by the sum of cross sections for double photoionization and ionization with excitation, because both these processes result in the formation of two vacancies in the $K$ shell. The universal scalings we obtained could be useful for analysis of such experiments [18].

## ACKNOWLEDGMENTS

We thank I. Bray and A. S. Kheifets for kindly supplying the results of their calculations in numerical form. Financial support from the RFBR under Grant No. 11-02-00943-a is also acknowledged.

## APPENDIX: CORRECTIONS TO FORMULAS IN REFS. [15] AND [16]

In Ref. [15], the amplitude $\mathcal{M}_d$ given by Eq. (44) contains a misprint. The correct expression reads

$$\mathcal{M}_d = -i(1-i\xi)D_\nu \int_0^1 \frac{dx}{\Lambda}\, x^{1-i/\beta} \left(\frac{\beta+\Lambda}{\beta+i}\right)^{2i/\beta} \times \frac{\partial}{\partial\nu}\frac{1}{(\nu-i\Lambda)}\frac{\partial}{\partial\nu}\frac{1}{(\nu-i\Lambda)^2} \times [Q_1(1) - Q_1(1+\nu-i\Lambda)]\big|_{\nu=n^{-1}},$$

where all notations are defined in the original paper [15].

In Ref. [16], there is an error in the amplitude $\mathcal{M}_c$. The correct function $P(x,y)$ given by Eq. (62) should read

$$P(x,y) = \frac{x(1-x)}{2\rho}\left[\frac{1}{\rho}+\frac{1}{\mu}+\frac{2(z-1)\sqrt{y}}{z^2+k^2}\right] + \frac{1}{\rho}\left(\frac{\rho-\nu}{q^2-\nu^2}\right)^2 + \frac{x^2(1-y)}{2\mu^2} + \frac{x^2\sqrt{y}}{\mu} \times \left[\frac{1-y}{(z-ik)^2} + \frac{(z-\varkappa y)}{z^2+k^2}\left(1-\frac{2}{z-ik}\right)\right],$$

where all notations correspond to the original work [16].

[1] J. H. McGuire, N. Berrah, R. J. Bartlett, J. A. R. Samson, J. A. Tanis, C. L. Cocke, and A. S. Schlachter, J. Phys. B **28**, 913 (1995).
[2] A. Müller, Adv. At. Mol. Opt. Phys. **55**, 293 (2008).
[3] R. Wehlitz, Adv. At. Mol. Opt. Phys. **58**, 1 (2010).
[4] M. Ya. Amusia, E. G. Drukarev, V. G. Gorshkov, and M. P. Kazachkov, J. Phys. B **8**, 1248 (1975).
[5] A. I. Mikhailov, I. A. Mikhailov, A. N. Moskalev, A. V. Nefiodov, G. Plunien, and G. Soff, Phys. Rev. A **69**, 032703 (2004).
[6] R. L. Brown, Phys. Rev. A **1**, 341 (1970).
[7] F. W. Byron Jr. and C. J. Joachain, Phys. Rev. **164**, 1 (1967).
[8] A. Dalgarno and H. R. Sadeghpour, Phys. Rev. A **46**, R3591 (1992).
[9] Z. Fan, H. R. Sadeghpour, and A. Dalgarno, Phys. Rev. A **50**, 3174 (1994).
[10] M. Ya. Amusia and A. I. Mikhailov, Zh. Eksp. Teor. Fiz. **111**, 862 (1997) [JETP **84**, 474 (1997)].
[11] E. G. Drukarev, E. Z. Liverts, M. Ya. Amusia, R. Krivec, and V. B. Mandelzweig, Phys. Rev. A **77**, 012715 (2008).
[12] J.-Z. Tang and J. Burgdörfer, J. Phys. B **30**, L523 (1997).
[13] A. S. Kheifets and I. Bray, Phys. Rev. A **58**, 4501 (1998).
[14] U. Kleiman, M. S. Pindzola, and F. Robicheaux, Phys. Rev. A **72**, 022707 (2005).

[15] A. I. Mikhailov and A. V. Nefiodov, Zh. Eksp. Teor. Fiz. **138**, 1028 (2010) [JETP **111**, 907 (2010)].
[16] A. I. Mikhailov and A. V. Nefiodov, Yad. Fiz. **74**, 207 (2011) [Phys. At. Nucl. **74**, 189 (2011)].
[17] S. M. Burkov, N. A. Letyaev, S. I. Strakhova, and T. M. Zajac, J. Phys. B **21**, 1195 (1988).
[18] A. I. Mikhailov, A. V. Nefiodov, and G. Plunien, J. Phys. B **42**, 231003 (2009).
[19] H. A. Bethe and E. E. Salpeter, *Quantum Mechanics of One- and Two-Electron Atoms* (Plenum, New York, 1977).
[20] T. Surić, E. G. Drukarev, and R. H. Pratt, Phys. Rev. A **67**, 022709 (2003).
[21] H. Bateman and A. Erdélyi, *Higher Transcendental Functions* (McGraw–Hill, New York, 1953), Vol. 1.
[22] V. B. Berestetskii, E. M. Lifshits, and L. P. Pitaevskii, *Quantum Electrodynamics* (Pergamon Press, London, 1982).
[23] E. P. Kanter, I. Ahmad, R. W. Dunford, D. S. Gemmell, B. Krässig, S. H. Southworth, and L. Young, Phys. Rev. A **73**, 022708 (2006).
[24] S. Huotari, K. Hämäläinen, R. Diamant, R. Sharon, C. C. Kao, and M. Deutsch, Phys. Rev. Lett. **101**, 043001 (2008).
[25] K. Fennane, J.-Cl. Dousse, J. Hoszowska, M. Berset, W. Cao, Y.-P. Maillard, J. Szlachetko, M. Szlachetko, and M. Kavčič, Phys. Rev. A **79**, 032708 (2009).
[26] J. Hoszowska, A. S. Kheifets, J.-Cl. Dousse, M. Berset, I. Bray, W. Cao, K. Fennane, Y. Kayser, M. Kavčič, J. Szlachetko, and M. Szlachetko, Phys. Rev. Lett. **102**, 073006 (2009).
[27] R. Wehlitz, I. A. Sellin, O. Hemmers, S. B. Whitfield, P. Glans, H. Wang, D. W. Lindle, B. Langer, N. Berrah, J. Viefhaus, and U. Becker, J. Phys. B **30**, L51 (1997).
[28] J. Mitdal, Phys. Rev. **138**, A1010 (1965).